

Voltage loss diagnosis in CO₂ electrolyzers using five-electrode technique

Kentaro U. Hansen

Luke H. Cherniack

*Feng Jiao**

Center for Catalytic Science and Technology, Department of Chemical and Biomolecular
Engineering, University of Delaware, Newark, DE 19716, USA.

AUTHOR INFORMATION

Corresponding Author

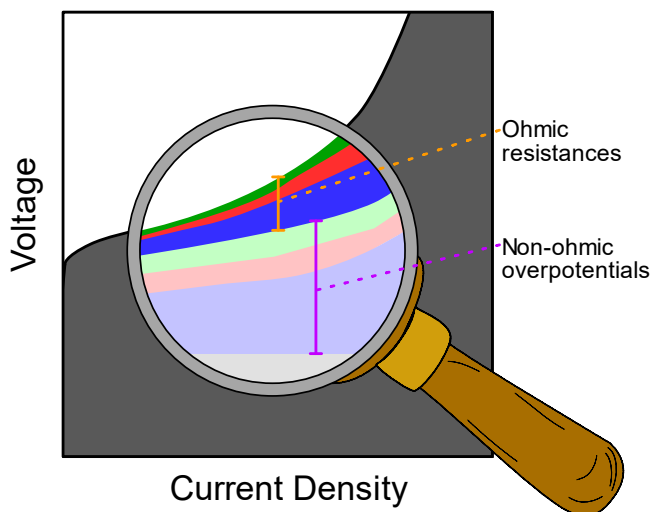
*jjiao@udel.edu

ABSTRACT

CO₂ electrolysis is a promising carbon utilization technology. Currently, energetic efficiency still requires a significant improvement for commercialization. To rationally design a more efficient CO₂ electrolyzer, diagnostic tools are necessary to pinpoint the source of voltage losses across the full cell at work. Here we develop a five-electrode technique to probe voltage drops at the cathode, anode, membrane and their interfaces in a typical zero-gap cell. We show that the

cathode/membrane ionic interface is the major source of overpotential, contributing 720 mV voltage loss at 600 mA cm⁻². This loss can be mitigated by coating the catalyst directly onto the membrane to lower ionic resistances, reducing this voltage loss to 80 mV at the same current density. The improved design enables us to achieve a full cell performance of 3.55 V and >95% CO Faradaic efficiency at 800 mA cm⁻² representing the highest performance for CO₂ electrolysis with a dilute bicarbonate electrolyte. The insights provided by the five-electrode technique may guide the rational design of future membrane-based electrochemical cells.

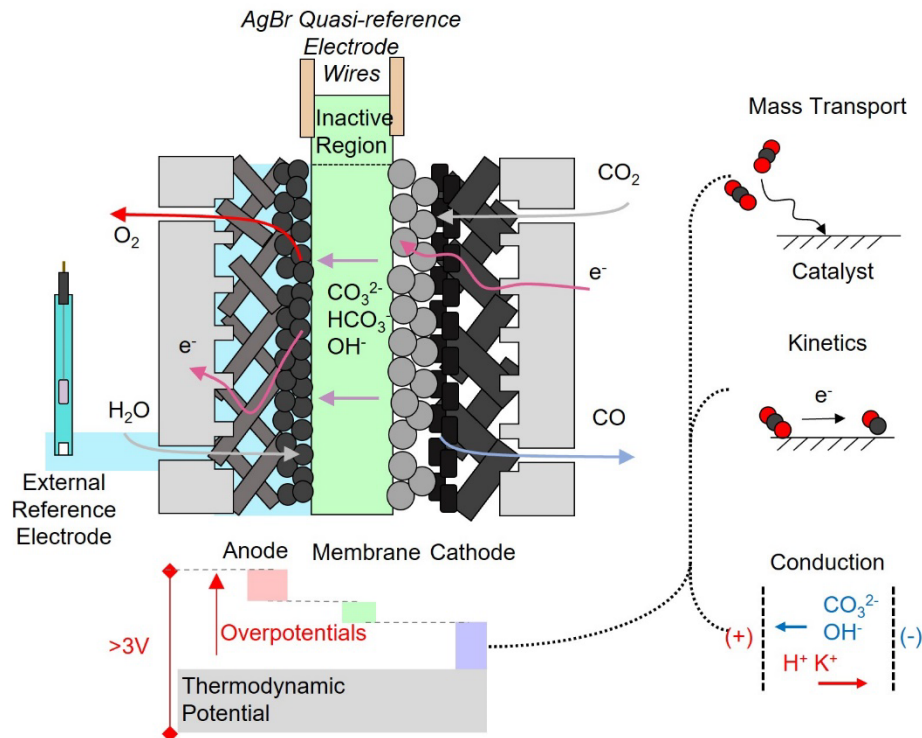
TOC GRAPHICS



MAIN TEXT

Carbon utilization technologies have the potential to offset costs of CO₂ capture while providing sustainable alternatives to fossil-fuel-derived products such as fuels and polymers. Low temperature (<100°C) CO₂ electrolysis is a promising carbon utilization technology to produce polymer and diesel precursors (ethylene, carbon monoxide), as well as liquid fuels (formic acid and ethanol)¹⁻³. In a typical CO₂ electrolyzer, electrochemical CO₂ reduction (CO₂R) occurs at the cathode (spanning 2 to 8 electrons per CO₂ molecule) while water or a fuel feedstock⁴⁻⁶ (e.g.,

hydrogen, glycerol) is oxidized at the anode with a polymer membrane between the electrodes to facilitate ion conduction. The most commercially relevant cell configuration for CO₂ electrolysis is a zero-gap configuration, where catalyst-coated substrates are compressed directly onto an ion-conducting polymer membrane (Scheme 1). Energetic efficiencies about 40%⁷⁻⁹ at industrially relevant current densities (>400 mA cm⁻²) has been achieved with zero-gap anion exchange membrane (AEM) configurations using commercially available high carbonate conductive membranes and ionomeric binders such as with Sustainion⁹⁻¹² (imidazolium-functionalized styrene) and Piperion^{8,13} (poly(aryl piperidinium)). Current research efforts primarily focus on improving individual components (catalysts, membranes) while achieving higher performance on a full device level remains challenging because the full cell performance is also impacted by factors beyond individual component properties under working conditions¹⁴. Thus, there is an urgent need to develop an operando tool to assess the performance of components and their interfaces at commercially relevant conditions to accelerate the development of CO₂ electrolysis for commercialization.



Scheme 1. Standard zero-gap configuration for CO₂ electroreduction to carbon monoxide with three reference electrodes. The total energy losses are related to the overpotential from each component. Overpotential can be broken down into three types: mass transport, kinetic, and conduction overpotential. Quasi-reference electrode wires are validated by open circuit potential measurement against the external reference electrode with the cell in an open circuit state.

The cell potential to drive CO₂ electrolysis is typically more than double the thermodynamic voltage arising from inefficiencies throughout the system. To better understand the source of these inefficiencies, the total cell potential can be derived from the sum of each component (Eqn 1). Under galvanostatic control, the potentials of the cathode ($E_{cathode}$), anode (E_{anode}) and membrane ($E_{membrane}$) can be measured by measuring the voltage drop between current collectors and reference electrodes pressed on the membrane (Eqn 1, Scheme 1). When the potential of the reference electrode under operating conditions are known, contributions from the expected

thermodynamic potential, E_{th} , and inefficiencies manifested as overpotentials, η , can be backed out (Eqn 2). Primary sources of overpotential in this system are related to ion/electron transport (η_{cond}), electrode kinetics (η_{kin}), and mass transport induced thermodynamic/kinetic effects (η_{mt}) (Eqn 3). Typically, ion/charge conduction overpotential both in the bulk and thin film electrolyte, generally established to be ohmic (R_{cond}) can be extracted with relative ease by measuring impedance at a fast frequency ($>10^3$ Hz)¹⁵⁻¹⁷. The combined kinetic/mass transport overpotential ($\eta_{non-ohmic}$) at the operating current density, i'' , can be evaluated by subtracting the ohmic resistance (Eqn 4). For generality, resistances are normalized to the active area of the electrode. There are several accounts where fritted reference electrodes and quasi-reference wires have been successfully contacted (directly or indirectly) to the membrane in fuel cells¹⁸⁻²¹, redox flow batteries²², and electrolyzers^{23,24} for CO₂ and H₂O. However, the techniques employed, such as using a flow field with a port for a leak-free reference electrode²⁴, membrane/wetted matrix (e.g., paper wipes) to extend the membrane out of the flow field²³, or sandwiching a reference electrode between a double membrane^{20,22}, lack flexibility in where the reference electrode outside of the active area of the electrochemical cell can be positioned (Figure S12). As such, convolution error where the probing point can be virtually located within the membrane rather than distinctly on the interfaces with the electrodes is difficult to control and mitigate.

$$E_{cell} = E_{cathode} - E_{anode} + E_{membrane} \quad (1)$$

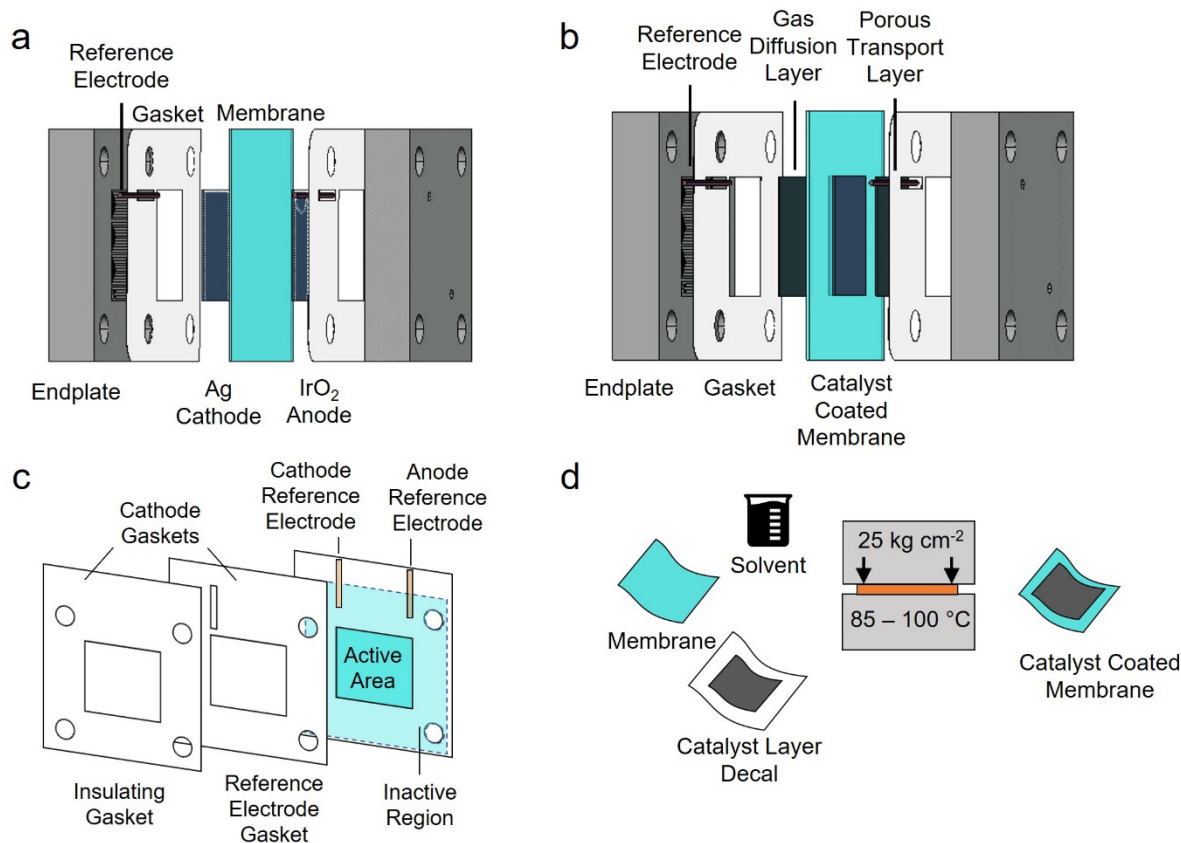
$$E_i = E_{i,th} + \eta_i \quad (2)$$

$$\eta_i = \eta_{i,kin} + \eta_{i,mt} + \eta_{i,cond} \quad (3)$$

$$\eta_{non-ohmic} = \eta_{i,kin} + \eta_{i,mt}, \eta_{cond} = i'' R_{cond} \quad (4)$$

To break down overpotentials for CO₂ electrolysis, we propose a 5-electrode (5E) measurement technique that addresses the issue of membrane convolution while providing better accessibility.

For the 5E measurement technique, two quasi-reference wires are introduced to the cell via gasket openings to inactive regions on each side of the membrane, enabling flexibility in the wire positioning that allows for leveraging optimal misalignment of electrodes to minimize convolution¹⁹ (Scheme 2a-c, Figure S11, Table S8). By selecting a reference wire thinner than the carbon paper or porous transport layer the original gasket can be substituted with two, one for placement of the wire and another for insulating the wire from the endplate. For the quasi-reference electrode wires, a stable, cheap and easy-to-fabricate silver-silver bromide redox couple (about 200 mV vs. 3.5M KCl Ag/AgCl) is selected and prepared via electrodeposition (Figures S1-S5, Tables S1-S3, See Supporting Information Section S1 for methods). A third external reference electrode, Ag/AgCl 3.5M KCl (Pine Research Instrumentation, Low Profile Silver Chloride (Ag/AgCl) Reference Electrode) is introduced to the anolyte fed to the cell for validation of the quasi-reference electrode wires. Further discussion about the technique is provided in Supporting Information Section S2. In total, a gasket substitution, two simple reference wires, and a multiplexer (or programmable relay box) are required to implement the technique (Figure S10). As shown in Figure S13, while operating under galvanostatic conditions, the connections to the reference and sense leads to each electrode is toggled via potentiostat programming to cyclically measure the voltage of each component. The minimal modifications to existing hardware make 5E measurements accessible with setups used for typical CO₂ electrolysis diagnostics.



Scheme 2. Key elements of the CO₂ electrolysis cell using a: a) zero-gap or b) catalyst coated membrane configuration. c) Schematic of AgBr quasi-reference electrode wire positioning on the membrane with accompanying gaskets.

We use this 5E measurement technique to benchmark the performance of a 5 cm² zero-gap configuration CO₂ electrolyzer by producing carbon monoxide as the primary product. Silver nanoparticles (Sigma Aldrich) was used as the cathode catalyst, Orion AMX 2.8 membrane (Orion Polymer) was used as the anion exchange membrane (AEM), and iridium oxide (Alfa Aesar) was used for the anode catalyst. (Tables S4-S6, Detailed methods are provided in Supporting Information Section S2). The resistance attributable to endplates and electrode support electronic conduction was evaluated for reference (Figures S8-S9). A pH meter (Apera Instruments PH8500) was used to monitor anolyte pH. Both the cell and electrolyte were heated to 40°C while

humidified (dew point = 35°C) CO₂ was fed in stoichiometric excess resulting in an outlet CO concentration of approximately 25%v/v.

Initially, the performance of the zero-gap configuration exhibited a cell potential of 3.58 V at 400 mA cm⁻² and poor Faradaic efficiency (<75%) towards CO at higher current densities (Figure 1a). Using 5E measurements, we can pinpoint that the critical bottleneck for this configuration is high cathode resistance comprising more than 66% of the total ohmic drop measured before the limiting current density. Thus, using the 5E measurement technique, we identified that to further reduce voltage drops in the cell, the optimization of cathode-membrane ion conduction should be prioritized.

Beyond discovering the cathode/membrane interface issue, direct measurement of the membrane potential during operation enables insightful benchmarking of membranes under practical operating conditions. As shown in Figure 1, the presence of a non-ohmic potential drop across the membrane, particularly for the zero-gap configuration, indicate that assuming a singular constant ionic resistance, which has been done in prior modeling work²⁵, is not necessarily valid for modeling voltammetric performance. Therefore, when ionic interfaces are poor, such as with dilute electrolyte and dry out effects, dynamic effects¹⁶ can play an outsized effect increasing the effective membrane resistance ($E_{membrane}/i'' > 1.0 \Omega \text{ cm}^2$) (Supporting Information Section S3, Figure S16) which needs to be considered when benchmarking or modeling membrane performance. Therefore, 5E measurements can help bridge learnings from ex situ polymer membrane studies to demonstration in electrolyzers by quantitating performance under harsh working conditions.

For AEM water electrolysis, catalyst coating the membrane rather than the porous electrode supports has been demonstrated to improve voltammetric performance, especially with either DI

water or dilute (<100mM) electrolytes²⁶). Improving ionic contact via CCM should have an outsized effect on CO₂ electrolysis performance since the membrane has an interfacial resistance increased by an order of magnitude in carbonated form (HCO₃⁻/CO₃²⁻) compared with the commonly reported resistance in hydroxide form (OH⁻)²⁷. Therefore, we aimed to hot-pressed catalyst coated membrane (CCM) configuration to mitigate poor cathode/membrane interfacial resistance (Scheme 2d, Figure S6, Table S7). By wetting the membrane with a H₂O: EtOH mixture, hot pressing with Orion AMX 2.8 was achieved at 100°C (Figure S7, Supporting Information Section S2).

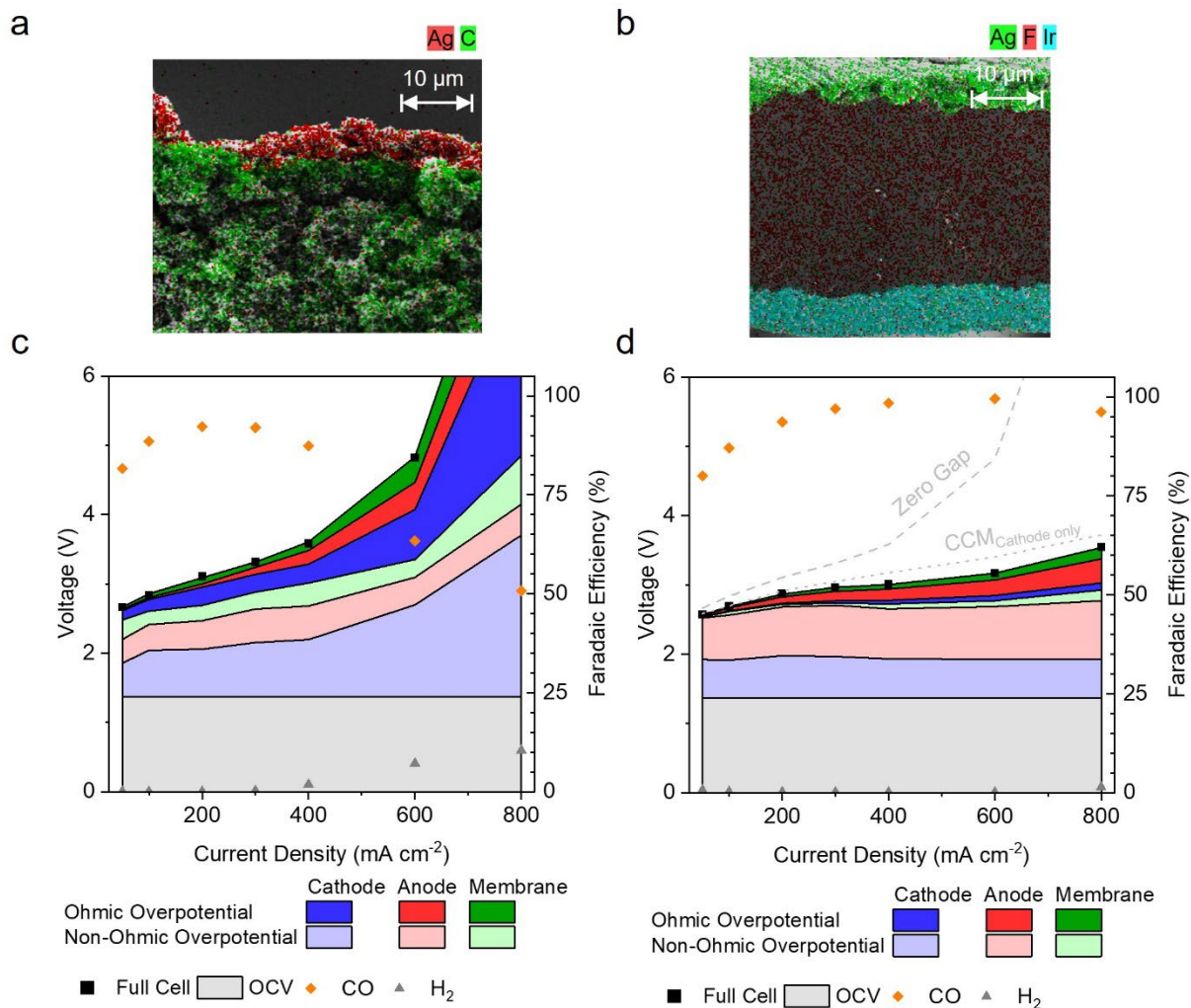


Figure 1. Scanning electron microscopy images of a) silver cathode on gas diffusion layer used in zero-gap configuration and b) Catalyst coated membrane (CCM) with elemental mapping. Voltammetric performance breakdown into ohmic and non-ohmic overpotentials for electrochemical CO₂ reduction to CO at 40°C for c) zero-gap configuration and d) CCM configuration using Orion AMX 2.8 as the anion exchange membrane with a recirculated CO₂ saturated 10 mM KHCO₃ anolyte. GC measurements were taken between ten to fifteen minutes into each current hold experiment.

This CCM configuration minimizes the cathode ohmic resistance, resulting in superb voltammetric performance where the cell potential at 400 mA cm⁻² is lowered by 0.57V (Figure 1d) with a reduction in the cathode resistance by 90%. Notably, the interface can be improved by other means, such as adding a concentrated liquid electrolyte^{26,28}. However, this would require further engineering of the cathode catalyst layer to avoid flooding due to salt precipitation²⁹ which is beyond the scope of this study. Overlaid in Figure 2b are the full cell potentials of zero-gap and cathode-only CCM configurations. The latter still exhibits most of the total performance benefit further supporting that the cathode-membrane interface, which is not exposed directly to 10mM electrolyte, is the critical interface. In conclusion, the CCM treatment uplifts the voltammetric performance to comparable with existing state of art performance for CO₂ electrolysis to CO within a range of ±0.1V at 400-800 mA cm⁻² under dilute/no supporting electrolyte <10mM KHCO₃ conditions^{7,13}.

We also compared zero-gap vs CCM performance for another AEM (FAA-3-50) with poor carbonate conductivity²⁷ in identical operating conditions (Supporting Information Section S4) to see if a similar trend could be observed. However, we only observed that ionic resistances shift from the cathode to the anode, indicating that not all AEMs may benefit from the CCM treatment

(Figure S19). We also benchmarked a CCM using a cation exchange membrane (CEM) with a porous anion-conducting layer between the cathode catalyst layer and the CEM because of its potential as an alternative to AEM-based configurations that mitigates issues such as the carbonation of anolyte or CO₂ release with anode tail gas^{30–33}. This configuration was diagnosed using 5E measurements. Initially, we found that depending on the identity of the CEM counterion (Na⁺, K⁺), the Faradaic efficiency of CO differed by more than 20% (Figure S20a-b). While total cell resistance and voltage were similar, the 5E technique revealed major differences in the distribution of ionic resistances throughout the cell (Figure S20c) which reflect the major changes that counter ion identity has on ionic resistance, water uptake, proton selectivity, electroosmotic drag of water across the membrane^{34,35}, that ultimately shape the microenvironment (i.e., pH, water) at the CO₂ reduction cathode beyond cation identity³⁶. While the exact mechanism by which counterion identity affects selectivity remains elusive here, it is our expectation that the 5E technique can provide the necessary optics to study complex behavior in a bipolar membrane configuration without a liquid electrolyte layer. In Table 1, we tabulate the discoveries made for the CO₂ electrolysis configurations using our probing technique. Ultimately, the 5E technique provides a new set of metrics for diagnosing a variety of CO₂ electrolysis cells beyond full cell potential and resistance.

Table 1. Summary of observations made for CO₂ electrolysis configurations

Configuration	Initial observation	5E Technique diagnosis
Orion AMX 2.8 AEM	Poor FE, high internal resistance when used in a zero-gap configuration	Cathode ionic resistance can be largely eliminated by catalyst coating the membrane
FAA-3-50 AEM	Poor FE, high internal resistance when used in both zero-gap and catalyst coated configurations	High ionic resistance is not eliminated but rather shifted to anode by catalyst coating the membrane

Nafion-Orion forward-bias BPM	Poor FE, when Nafion CEM is exchanged to K^+ form but FE improves when exchanged to Na^+ form despite similar total cell resistance.	High ionic resistance at anode shifts toward the cathode when changing Nafion CEM counterion from K^+ to Na^+
-------------------------------	--	---

Component-wise deconvolution through the 5E measurement also improves the effectiveness of electrochemical impedance spectroscopy (EIS) for understanding electrode dynamics in MEA configurations without a liquid electrolyte gap. Typically, EIS is only used qualitatively to understand zero-gap AEM performance because of the complexity of modeling the system with an equivalent circuit^{8,13}. Both the electrodes and the membrane have non-negligible contributions (>10%) to the full cell EIS which makes a causal link between an intervention and changes to impedance prone to error. More challenging, the timescale of phenomena that describe the impedance of each component are similar, which makes directly fitting the EIS data with parameters to describe each component an ill-posed problem. The 5E measurement technique addresses this issue by enabling the collection of three additional spectra for the cathode, anode, and membrane, which can be individually modeled and interpreted. However, the membrane impedance is not scrutinized further as there are nonlinear effects and other complexities that make spectra interpretation intractable without considerable physical modeling beyond the scope of this work¹⁶.

The impedance spectra for each electrode can then be interpreted by distributed relaxation times (DRT) analysis^{17,37}. DRT analysis enables quantitative comparisons between EIS results with more generalizability without presupposing a specific equivalent circuit. Specifically, DRT fits impedance data as an infinite series of capacitive and or inductive circuit elements which enables the sorting of internal resistance at an electrode that correspond to physical processes with varying time scales without necessitating the user to presuppose an equivalent circuit that might not

physically represent the electrode dynamics at play. EIS acquisition parameters and DRT fitting parameters used for this study are provided in Table S9 and Table S10 respectively. Figure 2b shows three distinct phenomena in the cathode EIS, which can be attributed to residual ionic/electronic conduction, electrode kinetics, and mass transport. As anticipated, the electrode kinetics resistance follows a Tafel relationship remarkably well (Supporting Information Section S3, Figure S18). Moreover, looking at the enhancement of not only ionic conduction but also charge transfer resistance at the cathode indicate that catalyst coating the membrane has a dual effect of improving catalyst utilization, which has been seen in AEM water electrolysis literature²⁶, on top of the order of magnitude improvement in ionic conductivity (Figure 2a). Surprisingly, the CCM configuration features higher ionic and charge transfer resistances at the anode rather than simply eliminating cathode resistances. Therefore, the benefit of implementing a CCM configuration is not as straightforward as initially expected. The missing Faradaic efficiency seen in the zero-gap configuration can be attributed to formate production³⁸. Formate is anionic species that can cross over an AEM and oxidize at the anode. In a separate experiment, we observed a reduction in the charge transfer resistance on the anode in the presence of potassium formate (Figure S21) due to the more facile oxidation of formate relative to water. Thus, we attribute the suppression of formate oxidation, by maintaining high FE towards CO, as the source of the higher anode charge transfer resistance seen in the CCM configuration. The deconvoluted electrode resistances can also be used to systematically model mass transport resistance exclusively at the cathode, which is exacerbated when approaching near unity single-pass conversion (Figure S17). Accordingly, coupling 5E measurements with EIS provides a path for decoupling electrode dynamics and membrane impedance to accelerate the development of more efficient components for CO₂ electrolysis.

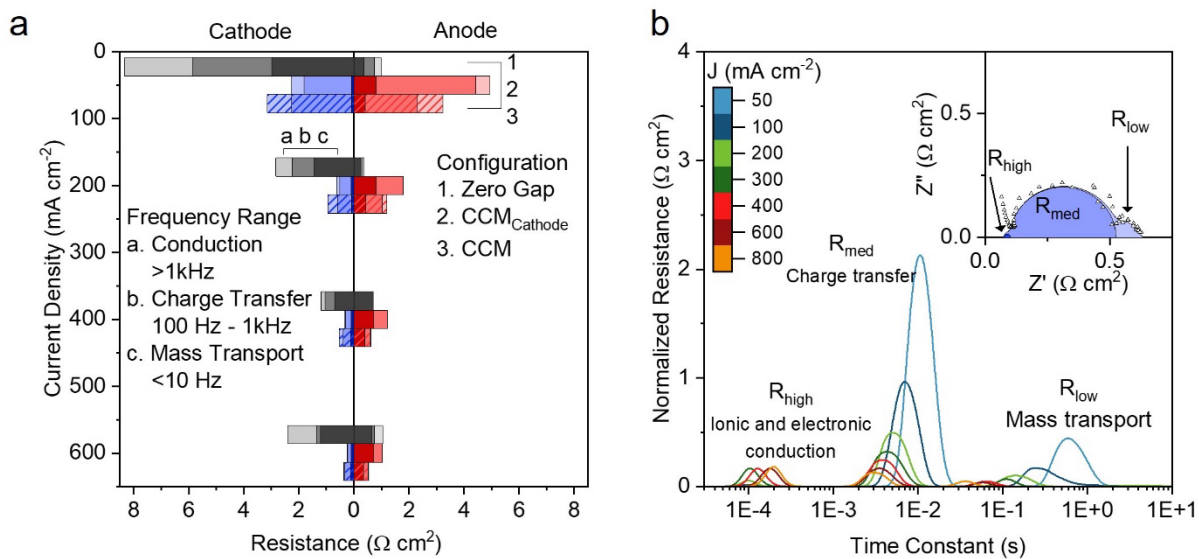


Figure 2. a) Cathode and anode resistances measured with electrochemical impedance spectroscopy and deconvoluted via Distributed Relaxation Times (DRT) methodology for zero-gap, fully catalyst coated membrane (CCM) and cathode-only coated membrane ($\text{CCM}_{\text{Cathode}}$) configurations. b) DRT results for cathode impedance taken for $\text{CCM}_{\text{Cathode}}$. Inset is the calculated Nyquist plot from the DRT results overlaid on experimental data obtained at 200 mA cm^{-2} .

Additionally, the 5E measurement technique can enrich the data collection for accelerated stability testing protocols. Accelerated stability testing is necessary for CO_2 electrolysis to meet expectations of durability and stability that make industrial application of this carbon utilization technology possible^{39,40}. Therefore, to understand the potential for the 5E measurement technique as a diagnostic aid, a pH failure diagnostic test was conducted using the cathode-only CCM configuration (Figure 3). The cell was cycled between 200, 800, and 0 mA cm^{-2} to make the most of EIS and validation capability gained by having an external reference electrode while still quickly instigating cell failure with the original testing configuration (Table 2). Without any interventions, the anode, followed quickly by the membrane and cathode, rapidly deteriorates after the anolyte hits a pH of 3. The anolyte composition drastically changed during operation; at the end of the test,

significant formate (21.2 mM) was detected via NMR, and only 10% of the initial K^+ concentration, with 8.7 μM of stainless-steel elements (Ni, Cr, Mo, Fe), was detected via ICPMS (Figure S14). EIS results (Figure 3b) further support that anode poisoning with these impurities led to a rapid increase in the ionic resistance leading to cell failure. Besides increased ionic resistance, increased kinetic resistance was observed due to 1.3 mg cm^{-2} of the initial 2.0 mg cm^{-2} of iridium oxide falling off the anode measured via XRF. To mitigate anode/anolyte degradation, the 50 mL anolyte reservoir was replenished with 10 mM KHCO_3 while removing well-mixed anolyte at a rate of 1 ml min^{-1} while the anode (with binder and IrO_2) was thermally annealed to limit IrO_2 losses. The result was stable short-term operation at 1 h intervals at 800 mA cm^{-2} as the pH saddled in the range of 5-6 (Faradaic efficiency measured throughout the duration of both tests are provided in Figure S15). While the original failure mechanism here was unmistakable from post-mortem observations, deconvolution still provides an opportunity to learn which components are stability-limiting during operation and can complement other measurements of stability such as FE and post-mortem characterizations.

Table 2. pH Failure diagnostic test current profile

Current Density (mA cm^{-2})	Duration (min)	Purpose
200	20	For acquiring clean and well-defined impedance data
0	0.033	To validate AgBr quasi-reference wire potentials with the external reference electrode throughout the test
800	60	To operate at the current density where instability is observed with the original testing configuration

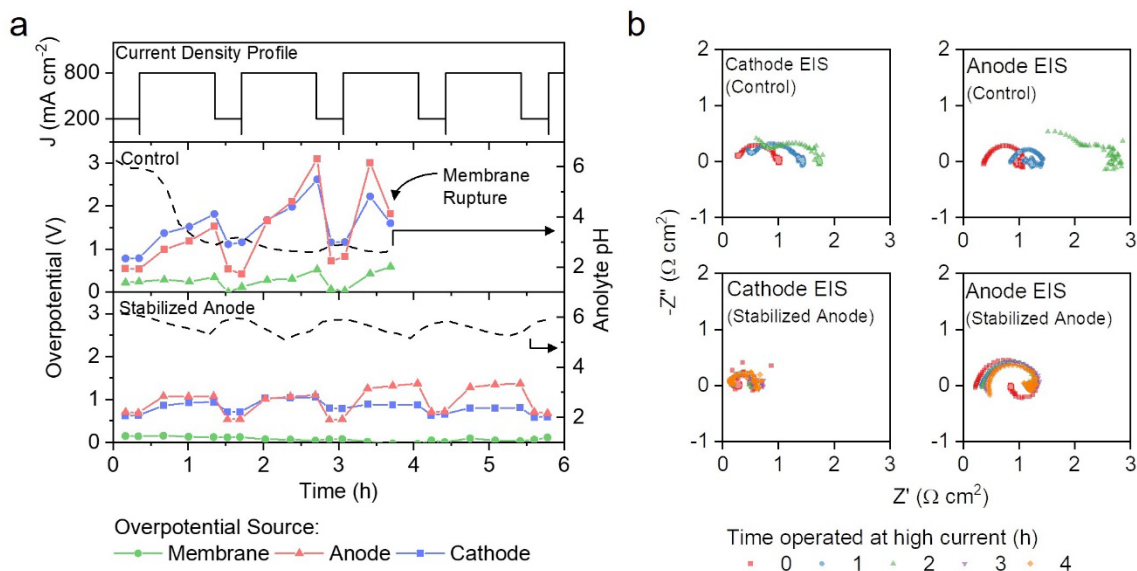


Figure 3. pH Failure diagnostic test of a cathode only catalyst-coated membrane configuration ($\text{CCM}_{\text{cathode}}$) using Orion AMX 2.8 (Control) and a modified $\text{CCM}_{\text{cathode}}$ with an annealed IrO_2 anode and anolyte (10 mM KHCO_3) replenishment (Stabilized anode). a) Overpotential traces and b) cathode and anode impedance taken at 200 mA cm^{-2} throughout the experiment.

In short, we developed a five-electrode measurement technique to rationally improve a CO_2 electrolyzer configuration and to enrich both EIS and stability testing methods. Using this technique, we identified poor ionic conductivity at the cathode-membrane interface that was then mitigated by catalyst-coating the membrane, thereby enabling high-performance CO_2 electrolysis with dilute electrolyte.^{18,19,21} The convenience of the technique, requiring only gasket modifications for the electrochemical cell, makes the impact of this work significant not only for CO_2 electrolysis but also as a general full device diagnostic platform for other membrane-based electrochemical systems.

ASSOCIATED CONTENT

Supporting Information. Experimental details on materials, quasi-reference electrodes, cell design, electrochemical techniques, additional experimental results and Supporting Information figures and tables

AUTHOR INFORMATION

Notes

Catalyst, membranes, and binder material for this study were purchased by the authors. The authors declare no competing financial interest.

ACKNOWLEDGMENT

The authors are grateful to the US Department of Energy for financial support (DE-EE0009287.0001). We thank Dr. Jong Yeob Jeon (Orion Polymer) for technical guidance with membrane hot pressing and Dr. Yong Zhao (University of Delaware) for help with scanning electron microscopy imaging.

REFERENCES

- (1) Jouny, M.; Luc, W.; Jiao, F. General Techno-Economic Analysis of CO₂ Electrolysis Systems. *Ind. Eng. Chem. Res.* **2018**, *57* (6), 2165–2177. DOI: 10.1021/acs.iecr.7b03514.
- (2) Chen, C.; Khosrowabadi Kotyk, J. F.; Sheehan, S. W. Progress toward Commercial Application of Electrochemical Carbon Dioxide Reduction. *Chem* **2018**, *4* (11), 2571–2586. DOI: 10.1016/j.chempr.2018.08.019.
- (3) De Luna, P.; Hahn, C.; Higgins, D.; Jaffer, S. A.; Jaramillo, T. F.; Sargent, E. H. What Would It Take for Renewably Powered Electrosynthesis to Displace Petrochemical Processes? *Science* **2019**, *364* (6438). DOI: 10.1126/science.aav3506.
- (4) Xia, C.; Zhu, P.; Jiang, Q.; Pan, Y.; Liang, W.; Stavitsk, E.; Alshareef, H. N.; Wang, H. Continuous Production of Pure Liquid Fuel Solutions via Electrocatalytic CO₂ Reduction Using Solid-Electrolyte Devices. *Nat. Energy* **2019**, *4* (9), 776–785. DOI: 10.1038/s41560-019-0451-x.
- (5) Verma, S.; Lu, S.; Kenis, P. J. A. Co-Electrolysis of CO₂ and Glycerol as a Pathway to Carbon Chemicals with Improved Technoeconomics Due to Low Electricity Consumption. *Nat. Energy* **2019**, *4* (6), 466–474. DOI: 10.1038/s41560-019-0374-6.
- (6) Xie, K.; Ozden, A.; Miao, R. K.; Li, Y.; Sinton, D.; Sargent, E. H. Eliminating the Need for Anodic Gas Separation in CO₂ Electroreduction Systems via Liquid-to-Liquid Anodic Upgrading. *Nat. Commun.* **2022**, *13* (1), 1–9. DOI: 10.1038/s41467-022-30677-x.
- (7) Yin, Z.; Peng, H.; Wei, X.; Zhou, H.; Gong, J.; Huai, M.; Xiao, L.; Wang, G.; Lu, J.; Zhuang, L. An Alkaline Polymer Electrolyte CO₂ Electrolyzer Operated with Pure Water. *Energy Environ. Sci.* **2019**, *12* (8), 2455–2462. DOI: 10.1039/c9ee01204d.

- (8) Endrődi, B.; Kecsenovity, E.; Samu, A.; Halmágyi, T.; Rojas-Carbonell, S.; Wang, L.; Yan, Y.; Janáky, C. High Carbonate Ion Conductance of a Robust PiperION Membrane Allows Industrial Current Density and Conversion in a Zero-Gap Carbon Dioxide Electrolyzer Cell. *Energy Environ. Sci.* **2020**, *13* (11), 4098–4105. DOI: 10.1039/d0ee02589e.
- (9) Liu, Z.; Yang, H.; Kutz, R.; Masel, R. I. CO₂ Electrolysis to CO and O₂ at High Selectivity, Stability and Efficiency Using Sustainion Membranes. *J. Electrochem. Soc.* **2018**, *165* (15), J3371–J3377. DOI: 10.1149/2.0501815jes.
- (10) Yang, H.; Kaczur, J. J.; Sajjad, S. D.; Masel, R. I. Electrochemical Conversion of CO₂ to Formic Acid Utilizing SustainionTM Membranes. *J. CO₂ Util.* **2017**, *20* (April), 208–217. DOI: 10.1016/j.jcou.2017.04.011.
- (11) Kaczur, J. J.; Yang, H.; Liu, Z.; Sajjad, S. D.; Masel, R. I. Carbon Dioxide and Water Electrolysis Using New Alkaline Stable Anion Membranes. *Front. Chem.* **2018**, *6* (JUL), 1–16. DOI: 10.3389/fchem.2018.00263.
- (12) Kutz, R. B.; Chen, Q.; Yang, H.; Sajjad, S. D.; Liu, Z.; Masel, R. I. Sustainion Imidazolium-Functionalized Polymers for Carbon Dioxide Electrolysis. *Energy Technol.* **2017**, *5* (6), 929–936. DOI: 10.1002/ente.201600636.
- (13) Endrődi, B.; Samu, A.; Kecsenovity, E.; Halmágyi, T.; Sebők, D.; Janáky, C. Operando Cathode Activation with Alkali Metal Cations for High Current Density Operation of Water-Fed Zero-Gap Carbon Dioxide Electrolysers. *Nat. Energy* **2021**, *6* (4), 439–448. DOI: 10.1038/s41560-021-00813-w.

(14) Lazaridis, T.; Stühmeier, B. M.; Gasteiger, H. A.; El-Sayed, H. A. Capabilities and Limitations of Rotating Disk Electrodes versus Membrane Electrode Assemblies in the Investigation of Electrocatalysts. *Nat. Catal.* **2022**, *5* (5), 363–373. DOI: 10.1038/s41929-022-00776-5.

(15) Wagner, N. Characterization of Membrane Electrode Assemblies in Polymer Electrolyte Fuel Cells Using a.c. Impedance Spectroscopy. *J. Appl. Electrochem.* **2002**, *32* (8), 859–863. DOI: 10.1023/A:1020551609230.

(16) Sistat, P.; Kozmai, A.; Pismenskaya, N.; Larchet, C.; Pourcelly, G.; Nikonenko, V. Low-Frequency Impedance of an Ion-Exchange Membrane System. *Electrochim. Acta* **2008**, *53* (22), 6380–6390. DOI: 10.1016/j.electacta.2008.04.041.

(17) Heinzmann, M.; Weber, A.; Ivers-Tiffée, E. Advanced Impedance Study of Polymer Electrolyte Membrane Single Cells by Means of Distribution of Relaxation Times. *J. Power Sources* **2018**, *402* (July), 24–33. DOI: 10.1016/j.jpowsour.2018.09.004.

(18) He, W.; Nguyen, T. Van. Edge Effects on Reference Electrode Measurements in PEM Fuel Cells. *J. Electrochem. Soc.* **2004**, *151* (2), A185. DOI: 10.1149/1.1634272.

(19) Zeng, R.; Slade, R. C. T.; Varcoe, J. R. An Experimental Study on the Placement of Reference Electrodes in Alkaline Polymer Electrolyte Membrane Fuel Cells. *Electrochim. Acta* **2010**, *56* (1), 607–619. DOI: 10.1016/j.electacta.2010.08.032.

(20) Sorsa, O.; Nieminen, J.; Kauranen, P.; Kallio, T. Stable Reference Electrode in Polymer Electrolyte Membrane Electrolyser for Three-Electrode Measurements. *J. Electrochem. Soc.* **2019**, *166* (16), F1326–F1336. DOI: 10.1149/2.0461916jes.

(21) Ohs, J. H.; Sauter, U.; Maass, S.; Stolten, D. The Effect of the Reference Electrode Position on the Measurement of Half Cell Polarization in Proton-Exchange Membrane Fuel Cells. *J. Electrochem. Soc.* **2012**, *159* (7), F181–F186. DOI: 10.1149/2.006207jes.

(22) Sun, C. N.; Delnick, F. M.; Aaron, D. S.; Papandrew, A. B.; Mench, M. M.; Zawodzinski, T. A. Probing Electrode Losses in All-Vanadium Redox Flow Batteries with Impedance Spectroscopy. *ECS Electrochem. Lett.* **2013**, *2* (5), 2013–2015. DOI: 10.1149/2.001305eel.

(23) Xu, Q.; Oener, S. Z.; Lindquist, G.; Jiang, H.; Li, C.; Boettcher, S. W. Integrated Reference Electrodes in Anion-Exchange-Membrane Electrolyzers: Impact of Stainless-Steel Gas-Diffusion Layers and Internal Mechanical Pressure. *ACS Energy Lett.* **2021**, *6* (2), 305–312. DOI: 10.1021/acseenergylett.0c02338.

(24) Salvatore, D.; Berlinguette, C. P. Voltage Matters When Reducing CO₂ in an Electrochemical Flow Cell. *ACS Energy Lett.* **2020**, *5* (1), 215–220. DOI: 10.1021/acseenergylett.9b02356.

(25) Weng, L. C.; Bell, A. T.; Weber, A. Z. Towards Membrane-Electrode Assembly Systems for CO₂ Reduction: A Modeling Study. *Energy Environ. Sci.* **2019**, *12* (6), 1950–1968. DOI: 10.1039/c9ee00909d.

(26) Park, J. E.; Kang, S. Y.; Oh, S. H.; Kim, J. K.; Lim, M. S.; Ahn, C. Y.; Cho, Y. H.; Sung, Y. E. High-Performance Anion-Exchange Membrane Water Electrolysis. *Electrochim. Acta* **2019**, *295*, 99–106. DOI: 10.1016/j.electacta.2018.10.143.

(27) Luo, X.; Rojas-Carbonell, S.; Yan, Y.; Kusoglu, A. Structure-Transport Relationships of Poly(Aryl Piperidinium) Anion-Exchange Membranes: Effect of Anions and Hydration. *J. Memb. Sci.* **2020**, *598* (August 2019), 117680. DOI: 10.1016/j.memsci.2019.117680.

(28) Mukundan, R.; Baker, A. M.; Kusoglu, A.; Beattie, P.; Knights, S.; Weber, A. Z.; Borup, R. L. Membrane Accelerated Stress Test Development for Polymer Electrolyte Fuel Cell Durability Validated Using Field and Drive Cycle Testing. *J. Electrochem. Soc.* **2018**, *165* (6), F3085–F3093. DOI: 10.1149/2.0101806jes.

(29) Leonard, M. E.; Clarke, L. E.; Forner-Cuenca, A.; Brown, S. M.; Brushett, F. R. Investigating Electrode Flooding in a Flowing Electrolyte, Gas-Fed Carbon Dioxide Electrolyzer. *ChemSusChem* **2020**, *13* (2), 400–411. DOI: 10.1002/cssc.201902547.

(30) Pătru, A.; Binninger, T.; Pribyl, B.; Schmidt, T. J. Design Principles of Bipolar Electrochemical Co-Electrolysis Cells for Efficient Reduction of Carbon Dioxide from Gas Phase at Low Temperature. *J. Electrochem. Soc.* **2019**, *166* (2), F34–F43. DOI: 10.1149/2.1221816jes.

(31) Xu Y, Miao RK, Jonathan P, Robb A, Sargent EH, Xu Y, Miao RK, Edwards JP, Liu S, Brien CPO, Gabardo CM, Fan M, Huang JE, Robb A, Sargent EH, Sinton D Article A microchanneled solid electrolyte for carbon- efficient CO₂ electrolysis A microchanneled solid electrolyte for carbon-efficient CO₂ electrolysis. :1–11. DOI: 10.1016/j.joule.2022.04.023

(32) O'Brien, C. P.; Miao, R. K.; Liu, S.; Xu, Y.; Lee, G.; Robb, A.; Huang, J. E.; Xie, K.; Bertens, K.; Gabardo, C. M.; et al. Single Pass CO₂ Conversion Exceeding 85% in the Electrosynthesis of Multicarbon Products via Local CO₂ Regeneration. *ACS Energy Lett.* **2021**, *6* (8), 2952–2959. DOI: 10.1021/acseenergylett.1c01122.

- (33) Ma, M.; Clark, E. L.; Therkildsen, K. T.; Dalsgaard, S.; Chorkendorff, I.; Seger, B. Insights into the Carbon Balance for CO₂ Electroreduction on Cu Using Gas Diffusion Electrode Reactor Designs. *Energy Environ. Sci.* **2020**, *13* (3), 977–985. DOI: 10.1039/d0ee00047g.
- (34) Shi, S.; Weber, A. Z.; Kusoglu, A. Structure-transport Relationship of Perfluorosulfonic-acid Membranes in Different Cationic Forms. *Electrochim. Acta* **2016**, *220*, 517–528. DOI: 10.1016/j.electacta.2016.10.096.
- (35) Okada, T.; Satou, H.; Okuno, M.; Yuasa, M. Ion and Water Transport Characteristics of Perfluorosulfonated Ionomer Membranes with H⁺ and Alkali Metal Cations. *J. Phys. Chem. B* **2002**, *106* (6), 1267–1273. DOI: 10.1021/jp013195l.
- (36) Hori, Y. Electrochemical CO₂ Reduction on Metal Electrodes. In *Modern Aspects of Electrochemistry*; 2008; pp 89–189. DOI: 10.1007/978-0-387-49489-0_3.
- (37) Wan, T. H.; Saccoccio, M.; Chen, C.; Ciucci, F. Influence of the Discretization Methods on the Distribution of Relaxation Times Deconvolution: Implementing Radial Basis Functions with DRTtools. *Electrochim. Acta* **2015**, *184*, 483–499. DOI: 10.1016/j.electacta.2015.09.097.
- (38) Larrazábal, G. O.; Strøm-Hansen, P.; Heli, J. P.; Zeiter, K.; Therkildsen, K. T.; Chorkendorff, I.; Seger, B. Analysis of Mass Flows and Membrane Cross-over in CO₂ Reduction at High Current Densities in an MEA-Type Electrolyzer. *ACS Appl. Mater. Interfaces* **2019**, *11* (44), 41281–41288. DOI: 10.1021/acsami.9b13081.
- (39) Nwabara, U. O.; De Heer, M. P.; Cofell, E. R.; Verma, S.; Negro, E.; Kenis, P. J. A. Towards Accelerated Durability Testing Protocols for CO₂ electrolysis. *J. Mater. Chem. A* **2020**, *8* (43), 22557–22571. DOI: 10.1039/d0ta08695a.

(40) Shin, H.; Hansen, K. U.; Jiao, F. Techno-Economic Assessment of Low-Temperature Carbon Dioxide Electrolysis. *Nat. Sustain.* **2021**, *4* (10), 911–919. DOI: 10.1038/s41893-021-00739-x.